Control of a Scaled Vehicle in and beyond Stable Limit Handling

Baars, Mart; Hellendoorn, Hans; Alirezaei, Mohsen

DOI
10.1109/TVT.2021.3085503

Publication date
2021

Document Version
Final published version

Published in
IEEE Transactions on Vehicular Technology

Control of a Scaled Vehicle in and Beyond Stable Limit Handling

Mart Baars, Hans Hellendoorn, and Mohsen Alirezaei

***Abstract*—In this research a controller is developed that can control path-tracking both within and beyond stable limit handling. The controller is based on the equations of motion of the nonlinear bicycle model. The performance of the controller is evaluated in simulation, a sensitivity analysis is performed and the controller is implemented on a 1/10 scale radio controlled car. The controller is able to track a path in normal driving conditions and let the vehicle enter and maintain a drift while remaining close to the desired path.**

***Index Terms*—Drift control, drifting, limit handling, scaled car.**

I. Introduction

AN AUTONOMOUS driving system should be able to control the vehicle in all driving situations, to ensure safety of the passengers. Especially controlling unstable behaviour, like drifting, is important since inappropriate control could have disastrous consequences. Being able to control this behaviour, however, does not only ensure safety but could also improve agility of the vehicle.

During typical cornering, the lateral motion of the vehicle is controlled by only the steering input [1]. During drifting, however, also the throttle input (on a rear-wheel driven car) has an influence on the lateral motion of the vehicle [1]. For this reason, a different control approach is required during drifting. In [1], a control approach is proposed that switches between two drift controllers; a steering focused controller that controls the drift by steering while keeping the rear longitudinal wheel slip constant and a throttle controller that keeps a constant steering input. Switching between those two controllers can prevent the vehicle from both spinning and exiting the drift in many situations. In [2] a linear quadratic MIMO controller is designed to control and stabilise a vehicle during steady-state drifting. In [3] a controller which mimics human driver for drifting is developed. the controller is consists of three consecutive layer where in upper layer the supervisor provides desired yaw rate and rear longitudinal slip ratio. In the second layer the desired lateral force and longitudinal forces are calculated for front and rear tyres, respectively and in the third layer the desired steering angle and gas pedal input are calculated. In [4] a Nonlinear Model Predictive Controller (NMPC) is used to find the steering and throttle input corresponding to a certain combination of tyre forces, that maintain the drift. By comparing predicted responses of different control inputs, an optimal input sequence can be estimated. A different control approach is presented in [5], [6], where the steering controller is equal for both typical cornering as for drift control. A path-tracking controller determines the steering input in both situations. The throttle input is based on longitudinal velocity for typical cornering and based on yaw rate, sideslip angle and longitudinal velocity during drifting. A State-Dependent Ricatti Equation (SDRE) controller is used to find the optimal controller gains.

Where the NMPC and SDRE controller show promising results, the complexity and the required computational resources for real-time application are a large drawback. The controller gains in [1] are mainly based on vehicle dynamics, this results in a simple and insightful controller that, in the basis, uses proportional control. Unlike the other two, this controller is unable to follow a path. Baars, Alirezaei and Hellendoorn [7] developed an extension to the work of Hindiyeh [1] by adding a path controller to the drift controller. A similar approach has been used in work of Goh [8]. In both research the way the path tracking added to the work of Hindiyeh is based on replacement of the equilibrium yaw rate with so called desired yaw rate. The desired yaw rate is calculated based on speed of the vehicle and curvature of the desired path. However, in this research the main contribution is in proposing a feedback-feedforward skim for the calculation of the desired curvature which is gradually converge to the curvature of the desired path, as described in [7], [9]. In which the proposed method includes path-tracking capabilities both within and beyond stable limit handling.

The research is structured as follows; In Section II the problem will be formulated. Next, the path-tracking and drifting errors will be defined in Section III. The design of the controller will be discussed in Section IV. The results based on simulations and implementation in a 1/10 scaled RC car will be analysed in Section V. In the final part of the paper conclusions will be drawn.

II. Problem Formulation

In normal driving conditions, a path can be tracked by using only the steering input of the vehicle. To maintain a drift,

Manuscript received July 7, 2020; revised December 12, 2020 and April 21, 2021; accepted May 5, 2021. Date of publication June 1, 2021; date of current version July 20, 2021. The review of this article was coordinated by Dr. Ricardo Pinto de Castro. *(Corresponding author: Mohsen Alirezaei.)*

Mart Baars is with the Department of Integrated Vehicle Safety, TNO, 5708 JZ Helmond, The Netherlands, and also with the Delft University of Technology, 2628 Delft, The Netherlands (e-mail: mart.baars@tno.nl).

Hans Hellendoorn is with the Delft University of Technology, 2628 Delft, The Netherlands (e-mail: J.Hellendoorn@tudelft.nl).

Mohsen Alirezaei is with the Siemens Industry Software and Services, 5708 JZ Helmond, The Netherlands, and also with the Eindhoven University of Technology, 5612 AZ Eindhoven, The Netherlands (e-mail: mohsen.alirezaei@siemens.com).

Digital Object Identifier 10.1109/TVT.2021.3085503

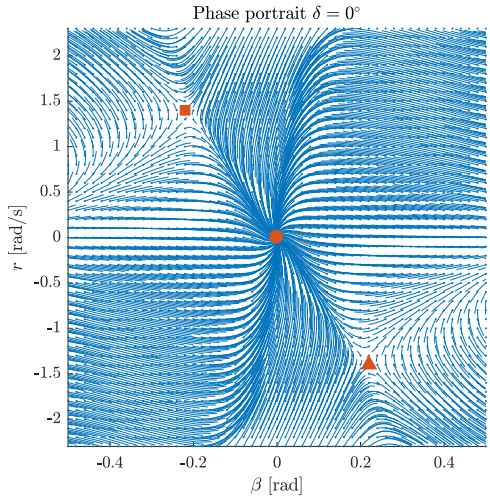

Fig. 1. Phase portrait for initial velocity $v = 1.5$ m/s and steering angle $\delta = 0°$. The markers show one stable (○) and two unstable equilibria (□, △).

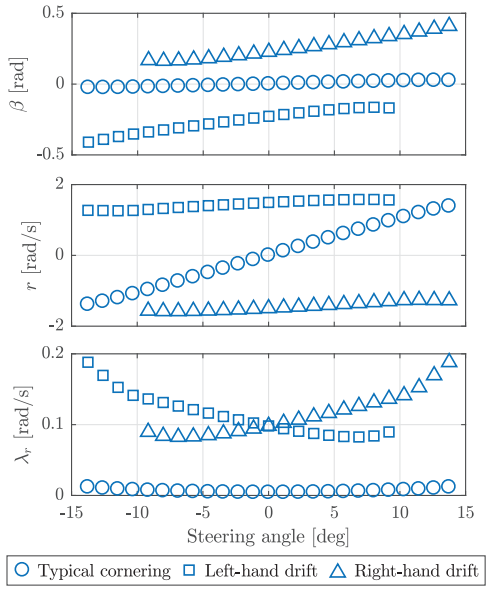

Fig. 2. Equilibrium analysis for $v = 1.8$ m/s. Showing the typical cornering and drift equilibria of the vehicle model for steering angles from -15 to $+15$ degrees.

however, control of the yaw motion and body sideslip angle of the vehicle is required. This requires simultaneous control of both the throttle and steering input. Since controlled drifting has an influence on both the lateral and longitudinal motion of the vehicle, path-tracking and drifting cannot be controlled as separate problems. A controller that combines both is therefore required. A seven degrees-of-freedom vehicle model of the 1/10 scaled RC car is used for development of the controller, where the seven degrees-of-freedom are the longitudinal, lateral and yaw motion, and the four wheel rotations. Other dynamics of the vehicle are neglected.

III. Equilibrium Analysis

The motion of a vehicle is highly non-linear, especially when large tyre slip occurs. To understand how a vehicle behaves in various driving scenarios, the phase trajectories for a range of initial sideslip angles, β, and yaw rates, r, for a fixed steering angle, δ, are observed. In Fig. 1 the phase trajectories for a steering angle of zero degrees are shown. The figure shows a minimum at the center (indicated by the ○), which represents straight-ahead driving and is a stable equilibrium. The two saddle points in the figure, indicated by the □ and △, are characterised by large sideslip angles and yaw rates. They represent unstable drift equilibria. The □ indicates a left-hand drift and the △ a right-hand drift.

For a change in steering angle or velocity, also the equilibria will change. An overview of the equilibria for various steering angles is shown in Fig. 2. The influence of the rear longitudinal wheel slip, λ_r, directly stands out, the wheel slips of all drift equilibria are much higher than for the typical cornering conditions, showing that the rear wheels in these equilibria are saturated. Furthermore, for a constant absolute velocity, a large range in equilibrium yaw rates is found. This means the trajectory can have a varying curvature, without having to change the velocity. This is convenient, since, due to the relationship between the longitudinal and lateral tyre force, the velocity is difficult to directly control during drifting. Moreover, the largest equilibrium yaw rate corresponds to a drift equilibrium. This means by drifting the vehicle can move in a sharper curvature than in typical cornering conditions.

IV. Error Definition

To design the drift controller first the error dynamics has to be defined. Based on the equilibria found in the previous section, the relationship between velocity, yaw rate, body sideslip angle and the required control inputs is known. By controlling the vehicle to the equilibrium states corresponding to a certain equilibrium point, a drift can be maintained. Therefore the errors are defined as

$$e_r = r - r^{eq}\ e_\beta = \beta - \beta^{eq}\ e_{v_x} = v_x - v_x^{eq} \tag{1}$$

Path-tracking also requires additional errors to control the position and heading of the vehicle with respect to the path. The error definition for path tracking is based on a widely used method as explained in [10], [11]. This method uses a look-ahead error, e_{la}, that needs to be minimized. The look-ahead error is the distance between the vehicle centreline and the tangent of the path at a look-ahead distance, x_{la}, in front of the vehicle. The definition of the look-ahead error is given by

$$e_{la} = y_e + x_{la}\sin(\psi_e), \tag{2}$$

where y_e is the lateral distance from the Centre of Gravity of the vehicle to the path, x_{la} is the look-ahead distance and ψ_e is the heading error, the angle between the centreline of the vehicle and the path tangent. At high body sideslip manoeuvres, the look-ahead definition from Eq. (2) causes two problems, both caused by the assumption of a small body sideslip angle. The first problem arises at the measurement of the lateral error. At large body sideslip angles, the distance to a point on the path

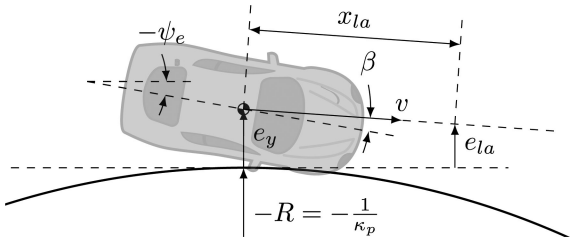

Fig. 3. Path-tracking error definition as used in this research, where β is the sideslip angle, e_{la} is the look-ahead error, e_y is the lateral error, ψ_e is the heading error, κ_p is the path curvature, R is the path radius, v is the vehicle longitudinal velocity and x_{la} is the look-ahead distance.

lateral to the vehicle is not representative for the distance to the path. The shortest distance from the vehicle to a point on the path is a better measure. Secondly, the look-ahead error is based on the heading of the vehicle only. During drifting the heading of the vehicle is not equal to the direction of motion of the vehicle, which is approximately the case in typical cornering conditions. Therefore, in these conditions, the body sideslip angle needs to be taken into account in the definition of the look-ahead error. Since, however, direct input of the sideslip angle results in reduced stability margins and yaw oscillations at high lateral accelerations, a predicted steady-state body sideslip angle, β_{ss}, is used [12]. The steady-state body sideslip angle is given by

$$\beta_{SS} = \left(\frac{mav_x^2}{\ell C_{\alpha,r}} - b \right) \kappa_p, \tag{3}$$

where, m is the vehicle mass, a is the distance from the centre of gravity to the front wheels, $C_{\alpha,r}$ is the rear tyre cornering stiffness, ℓ is the wheelbase and κ_p is the reference path curvature. The resulting look-ahead error definition, as used in this research, is given by

$$e_{la} = e_y + x_{la} \sin(\psi_e + \beta_{ss}) \tag{4}$$

and visualised in Fig. 3.

V. Controller Structure

The response of the vehicle to steering and throttle inputs differs in typical cornering conditions and for large body sideslip manoeuvres [1]. For that reason, a separate controller for both conditions is used. A schematic of the controller structure is shown in Fig. 4.

The reference generator uses path information (curvature and path-tracking errors) from the positioning system and the vehicle states, $\mathbf{x}$, to select a controller and define the state references, $\mathbf{r}$. Selection of the controller is based on the equilibria found in Section III.

The output of both the typical cornering and drift controller are a steering input (u_s) and a desired longitudinal wheel slip. A low-level longitudinal wheel slip controller is used to handle the nonlinear dynamics of the drive line. The output of the controller is a throttle input (u_t) that can directly be fed into the vehicle.

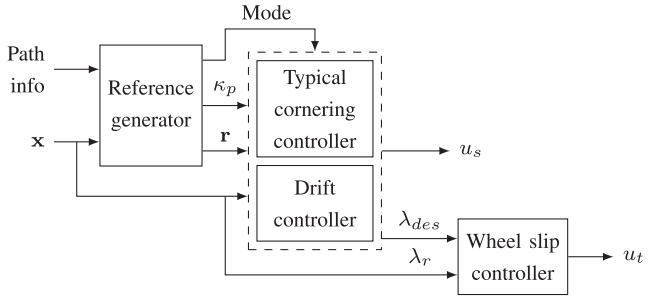

Fig. 4. Schematic of the main controller structure. The reference generator creates the reference and decides on the controller mode (typical cornering or drifting) based on path and vehicle state information. The wheel slip controller is the engine controller that controls the engine speed to reach the desired rear wheel slip.

A. Typical Cornering

In typical cornering conditions the steering angle and throttle input both have control authority over different driving tasks. The steering input is used for lateral control and the throttle input for longitudinal control. Path tracking can, therefore, be achieved by controlling the steering angle only. The throttle input is used to maintain the desired velocity.

The lateral control approach used in this research is based on [13]. A combination of feedforward and feedback is used to minimize the path-tracking errors as defined in Section IV. The steering command is given by

$$u_s = \delta_{FF} + \delta_{FB}, \tag{5}$$

where δ_{FF} and δ_{FB} denote feedforward and feedback steering angle respectively. The feedforward steering angle is obtained with

$$\delta_{FF} = \left(\ell + K_{us} v_x^2 \right) \kappa, \tag{6}$$

where $K_{us} = \frac{m_f}{C_{\alpha,f}} - \frac{m_r}{C_{\alpha,r}}$ is the understeer gradient. Where m_f and m_r are the front and rear load respecively. This controller is based on vehicle kinematics and steady-state cornering [13], [14]. The feedback controller is based on the same equation, but with a feedback curvature based on the look-ahead error. The look-ahead error can be seen as Sagitta of a circle with radius $\frac{1}{\kappa_{FB}}$. The feedback curvature can then be found by

$$\kappa_{FB} = -\frac{2e_{la}}{e_{la}^2 + (x_{la} + b)^2} \approx -\frac{2e_{la}}{(x_{la} + b)^2}, \tag{7}$$

where the look-ahead distance in the denominator can be neglected since it is small compared to the radius of the circle. Note that in this equation the curvature starts at the rear axle, since it can be assumed that there is no lateral motion at the rear axle in typical cornering conditions (no slip). The resulting feedback steering angle is defined by

$$\begin{aligned} \delta_{FB} &= \left(\ell + \frac{K_{us} v_x^2}{g} \right) \kappa_{FB} \\ &= -\left(\ell + \frac{K_{us} v_x^2}{g} \right) \frac{2(e_y + x_{la} \sin(\psi_e + \beta_{ss}))}{(x_{la} + b)^2}. \end{aligned} \tag{8}$$

A human driver will look further ahead if driving at a higher velocity. For that reason, the look-ahead distance is also made dependent on velocity

$$x_{la} = vt_{la}, \tag{9}$$

where t_{la} is the look-ahead time.

B. Limit Handling

During high body sideslip manoeuvres, the vehicles lateral and yaw motion are controlled by the steering and motor input simultaneously. This, however, requires an input coordination scheme. Hindiyeh showed that it is possible to maintain a drift by controlling either one of the control inputs and keeping the other at its equilibrium state [1]. A combination of both controllers, based on the equations of motion of the bicycle model, is used to develop the coordination scheme [1].

1) Controller Definition: In Eq. (10) the lateral equations of motion of the bicycle model are shown. Both the yaw and sideslip dynamics have a dependency on the front and rear lateral tyre forces:

$$\dot{\beta} = \frac{F_{y,f} + F_{y,r}}{mv_x} - r, \tag{10a}$$

$$\dot{r} = \frac{aF_{y,f} - bF_{y,r}}{I_z}. \tag{10b}$$

These equations show that the front and rear lateral tyre forces influence the yaw and body sideslip motion. The magnitude and sign of a lateral tyre force, depend on the wheel slip angle. For the front wheels, the wheel slip angle can easily be changed by changing the steering angle. For the rear wheels however, only the longitudinal wheel slip can be controlled directly. This makes it difficult to change the sign of the rear lateral tyre force. The body sideslip dynamics (Eq. (10a)) are also controlled by the yaw rate, since the vehicle has to rotate to get to a certain body sideslip angle. Hindiyeh, therefore, proposes to control the body sideslip angle via the yaw rate. The controller therefore contains an outer loop, that defines a desired yaw rate based on the body sideslip angle error, and an inner loop that controls the vehicle to this desired yaw rate. The outer loop of the controller is defined by

$$r_{des} = r^{eq} + K_\beta e_\beta, \tag{11}$$

where r^{eq} is the yaw rate of a certain drift equilibrium, K_β is the sideslip error feedback gain and e_β is the sideslip error:

$$e_\beta = \beta - \beta^{eq}. \tag{12}$$

The inner loop is found by feedback linearization of the yaw rate error:

$$\dot{e}_r = \dot{r} - \dot{r}_{des} = -K_r e_r, \tag{13}$$

where K_r is the yaw rate error feedback gain and $e_r = r - r^{eq}$ is the yaw rate error. Substitution of the derivative of the desired yaw rate,

$$\dot{r}_{des} = K_\beta \dot{e}_\beta \tag{14}$$

$$= K_\beta \dot{\beta}, \tag{15}$$

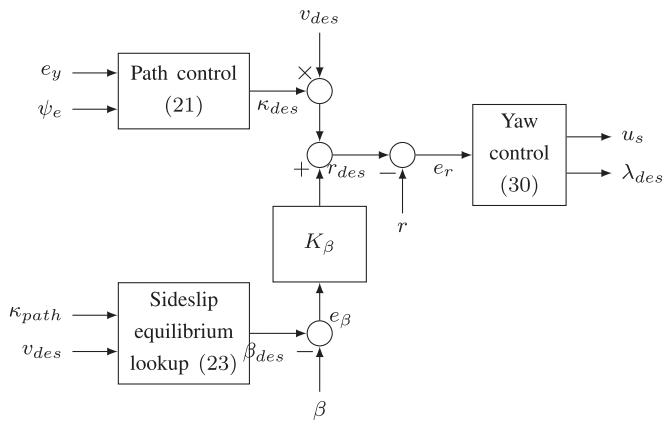

Fig. 5. Schematic of the drift controller structure. The path controller and Sideslip equilibrium lookup together result in a desired yaw rate. The yaw rate controller controls the vehicle to achieve this yaw rate. The numbers in the controller blocks are the equation numbers.

in 13 results in:

$$\dot{r} - K_\beta \dot{\beta} = -K_r e_r. \tag{16}$$

Substitution of the lateral equations of motion (Equation 10) results in:

$$\frac{aF_{y,f} - bF_{y,r}}{I_z} - K_\beta \left(\frac{F_{y,f} + F_{y,r}}{mv_x} - r \right) = -K_r e_r. \tag{17}$$

Collection of the lateral tyre forces results in

$$\left(\frac{a}{I_z} - \frac{K_\beta}{mv_x} \right) F_{y,f} - \left(\frac{b}{I_z} + \frac{K_\beta}{mv_x} \right) F_{y,r}$$

$$= -(K_\beta + K_r) r + K_r r^{eq} + K_\beta K_r (\beta - \beta^{eq}). \tag{18}$$

This equation represents the required combination of the front and rear lateral tyre forces to minimise the yaw rate and sideslip error and maintain at the drift equilibrium. This controller is the basis for the path-tracking drift controller developed in this research.

To add path tracking capabilities to this basic drift controller, the reference yaw rate, r^{eq}, and body sideslip angle, β^{eq}, in Eq. (18) are exchanged by a yaw rate and body sideslip angle based on the path curvature and path-tracking errors, $r_{des,pt}$ and $\beta_{des,pt}$. The resulting controller structure is shown in Fig. 5, where the inner loop contains the yaw control on the right and the outer loop contains the path and sideslip control [7]. The desired yaw rate is obtained by multiplication of a desired curvature and a desired velocity, where the desired curvature is derived from the path-tracking errors. The derivation of the desired yaw rate is given as follows:

$$r_{des,pt} = \kappa_{des} v_{des}, \tag{19}$$

The desired curvature consists of a feedforward and feedback curvature:

$$\kappa_{des} = \kappa_{FF} + \kappa_{FB}, \tag{20}$$

where the feedforward curvature, κ_{FF}, is equal to the path curvature. Similar to the typical cornering conditions, the feedback

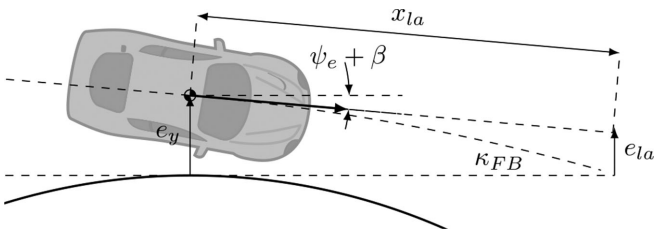

Fig. 6. The feedback-curvature, κ_{FB}, based on the look-ahead error, e_{la}.

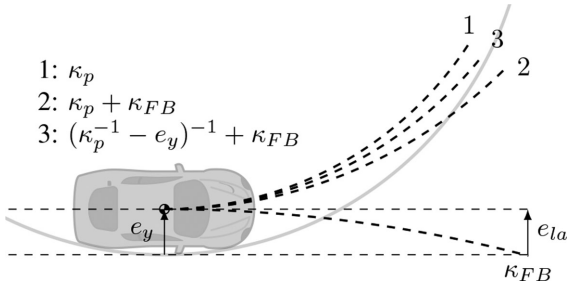

Fig. 7. Comparison between two definitions of the desired curvature, with (1) the path curvature, (2) the desired curvature, as used in the typical cornering conditions, and (3) the desired curvature used in drift conditions

curvature is the curvature to drive to resolve the path tracking errors, as shown in Fig. 6. During drifting, however, the path tracking errors are calculated with respect to the centre of gravity, since the vehicle rotates around this point. Similar to Eq. (7) the feedback curvature is calculated by:

$$\kappa_{FB} = -\frac{2e_{la}}{e_{la}^2 + x_{la}^2} \approx -\frac{2e_{la}}{x_{la}^2}. \tag{21}$$

Plugging this feedback curvature into Eq. (20) and using the path curvature as feed forward, results in the following desired curvature definition:

$$\kappa_{des} = \kappa_p - \frac{2e_{la}}{x_{la}^2}. \tag{22}$$

In Fig. 7 this definition of the desired curvature is visualised (curve 2), compared to the path curvature (curve 1). The figure shows that curve 2 will result in an overshoot, since the reaction is too severe. This figure also shows that the path curvature as feed forward already resolves the path-tracking errors partly. To improve desired curvature definition, an adaption is proposed:

$$\kappa_{des} = (\kappa_p^{-1} - e_y)^{-1} - \frac{2e_{la}}{x_{la}^2}. \tag{23}$$

In this definition, the radius of the path is reduced by the lateral error. This results in a desired curvature that brings the vehicle closer to the path, without crossing the path (curve 3 in Fig. 7.

The next step to incorporate the path tracking errors in the drift controller from Eq. (18) is to define the desired body sideslip angle, $\beta_{des,pt}$, based on the path information. From Fig. 2 it can be observed that the relationship between the equilibrium yaw rate and equilibrium sideslip angle is approximately linear. The equilibrium body sideslip angle in Eq. (18) is, therefore, defined as a function of the equilibrium yaw rate:

$$\beta^{eq} = f_{\beta^{eq}}(r^{eq}). \tag{24}$$

The required equilibrium yaw rate can be obtained from the path information and path tracking errors. However, basing the body sideslip angle on path-tracking errors results in undesired behaviour of the controller. A higher equilibrium yaw rate corresponds to a smaller (less negative) equilibrium sideslip angle (Fig. 2), but to rotate to a smaller body sideslip angle, the yaw rate needs to decrease. Since these opposite influences are undesired, the reference body sideslip angle is selected only from the curvature of the path:

$$\beta_{des,pt} = f_{\beta^{eq}}(\kappa_p v_{des}). \tag{25}$$

With the definition of $r_{des,pt}$ and $\beta_{des,pt}$ based on the path tracking errors, now the drift controller from Eq. (18) can be derived again. The equilibrium states r^{eq} and β^{eq} from Eq. (11) and Eq. (12) will be interchanged with the desired states $r_{des,pt}$ and $\beta_{des,pt}$, resulting in the following equations:

$$r_{des} = \kappa_{des} v_{des} + K_\beta e_\beta. \tag{26}$$

$$e_\beta = \beta - f_{\beta^{eq}}(\kappa_p v_{des}) \tag{27}$$

$$\dot{r}_{des} = \dot{\kappa}_{des} v_{des} - K_\beta(\dot{\beta} - \dot{\beta}_{des}) \tag{28}$$

where $\dot{\kappa}_{des}$ is defined as:

$$\dot{\kappa}_{des} = \frac{\dot{\kappa}_p + v\sin(\psi_e + \beta)\kappa_p^2}{(1 - e_y\kappa_p)^2} - \frac{2}{x_{la}^2}\dot{e}_{la} \tag{29}$$

and $\dot{\beta}_{des}$ is defined as:

$$\dot{\beta}_{des} = f'_{\beta^{eq}}(\kappa_p v_{des})\dot{\kappa}_p v_{des}. \tag{30}$$

These equations describe the outer loop of the drift controller with path-tracking capabilities. With this definition, the proposed controller equation can be derived as is done in Eq. (11) to Eq. (18).

Substituting Eq. (28) in the inner loop of the drift controller from Eq. (13) results in:

$$\dot{e}_r = \dot{r} - \dot{\kappa}_{des} v_{des} - K_\beta(\dot{\beta} - \dot{\beta}_{des}) = -K_r(r - r_{des}). \tag{31}$$

Substitution of the lateral equations of motion (Eq. (10)) results in:

$$\frac{aF_{y,f} - bF_{y,r}}{I_z} - K_\beta\left(\frac{F_{y,f} + F_{y,r}}{mv_x}\right) = \dot{\kappa}_{des} v_{des} - (K_\beta + K_r)r - K_r r_{des} - K_\beta\dot{\beta}_{des} \tag{32}$$

Substitution of Eq. (29) and Eq. (30) and collection of the lateral tyre forces results in:

$$K_{F_{y,f}}F_{y,f} - K_{F_{y,r}}F_{y,r} = \left(\frac{\kappa_p^2 v}{(1 - e_y\kappa_p)^2} - \frac{2v}{x_{la}^2} + K_r\frac{2}{x_{la}}\right) v_{des}\sin(\psi_e + \beta)$$

$$- K_r \left(\frac{\kappa_p}{1 - e_y \kappa_p} - \frac{2e_y}{x_{la}^2} \right) v_{des} - (K_\beta + K_r) r$$
$$- \frac{2\kappa_p v \cos^2(\psi_e + \beta)}{x_{la}^2} v_{des} + \left(\frac{1}{(1 - e_y \kappa_p)^2} - K_\beta f'_{\beta^{eq}} \right) \dot{\kappa}_p v_{des} \tag{33}$$

with

$$K_{F_{y,f}} = \frac{a}{I_z} - \frac{K_\beta}{m v_x} + \frac{2 v_{des}}{m v_x x_{la}} \cos(\psi_e + \beta)$$

and

$$K_{F_{y,r}} = \frac{b}{I_z} + \frac{K_\beta}{m v_x} - \frac{2 v_{des}}{m v_x x_{la}} \cos(\psi_e + \beta).$$

2) Control Input Coordination: The resulting controller equation (Eq. (33)) determines a combination of the front and rear lateral tyre forces, required to minimise the yaw rate, body sideslip angle and path-tracking errors. To calculate the separate tyre forces, however, the value of one of the tyre forces is required. Hindiyeh uses two controller modes to find the separate tyre forces; a steering mode and a throttle mode [1]. These controller modes are adjusted to work with the addition of path-tracking capabilities.

Steering mode: The steering mode is the initial mode of the controller. In this mode, the steering angle is used to control the drift and the throttle input to control the longitudinal velocity of the vehicle. The following steps are taken to find the lateral tyre forces:

1) A desired rear longitudinal wheel slip is calculated to keep the velocity and body sideslip angle constant:

$$\lambda_{des} = \lambda^{eq} + K_{v,t}(v_{des} - v) + K_{r,t} e_{r,t}., \tag{34}$$

where t denotes throttle control and

$$e_{r,throttle} = \begin{cases} r_{des,t} - r & \text{if} \quad r_{des,t} \geq 0 \\ r - r_{des,t} & \text{if} \quad r_{des,t} < 0 \end{cases} \tag{35}$$

with

$$r_{des,t} = r^{eq} + K_{\beta,t} e_\beta, \tag{36}$$
$$= \kappa_p v_{des} + K_{\beta,t}(\beta - f_{\beta^{eq}}(\kappa_p v_{des}). \tag{37}$$

Note that in this desired yaw rate calculation only the sideslip error, velocity and path curvature are taken into account, not the path-tracking errors. This is to make sure the rear wheel slip remains high enough to keep the vehicle in a drift.

2) With this rear longitudinal wheel slip, the rear lateral tyre force is calculated:

$$F_{y,r} = f_{t,r}(\lambda_{des}, \alpha_r, F_{z,r}). \tag{38}$$

3) Inserting the rear lateral tyre force in Eq. (33) results in the front lateral tyre force.
4) From the front lateral tyre force a desired steering angle is calculated:

$$u_s = f_{t,f}^{-1}(F_{y,f}, \lambda_f, F_{z,f}) + \arctan\left(\beta + \frac{ar}{v_x}\right). \tag{39}$$

If the lateral tyre force cannot be reached, the maximum reachable front lateral tyre force is used and the controller switches to throttle mode.

Throttle mode: These steps are only taken when the front tyre reaches its force limit.

1) With the determined maximum front lateral tyre force and Eq. (33) a new rear lateral tyre force is calculated.
2) With the new rear lateral tyre force a new desired longitudinal wheel slip is determined:

$$\lambda_{des} = f_{t,r}^{-1}(F_{y,r}, \alpha_r, F_{z,r}). \tag{40}$$

By following the above steps, the controller is able to stabilize the vehicle in a large range of equilibrium states and for fairly significant friction variations. Since the controller most of the time operates in steering mode, the velocity remains fairly constant. When in danger of exiting the drift, however, the velocity error is temporarily sacrificed to maintain the drift.

VI. Sensitivity Analysis

The controller gains are found to keep the vehicle at the reference equilibrium. But, the controller should be able to stabilise the vehicle when the states are not exactly at their equilibrium value. A sensitivity analysis is performed to test the performance of the controller around the reference equilibrium. In this analysis, the sensitivity of the controller to changes in initial conditions, reference values or model parameters is analysed.

A. Initial Path-Tracking Errors

First, the ability of the controller to return the vehicle to the path, if initialised with a lateral or course offset, is analysed. Multiple simulations are performed with the lateral error varied between ± 0.3 m and the course error between ± 0.15 rad. Note that 0.3 m offset is about 100% of the wheel base of the vehicle and therefore is a considerable disturbance to the system. Other vehicle states are unchanged and correspond to the reference equilibrium point. In Fig. 8 a phase portrait is shown. This phase portrait gives insight in how the controller is able to solve path tracking errors. The orange dots are the initial path-tracking errors where the simulation is started. From the figure it becomes apparent that the path-tracking errors are resolved in a spiral motion. To minimise a lateral error, the vehicle has to move towards the path. Moving towards the path means that the course of the vehicle (direction of motion, $\psi + \beta$) does not align with the path tangent. So to decrease the lateral error, first the course error will increase. This results in the spiral-shaped phase portrait. For the offsets shown in the figure, the controller is able to stabilise the vehicle at the reference equilibrium in approximately 2 to 7 seconds, as can be seen in Fig. 9, depending on the magnitude of the initial errors. In most cases though, the errors are resolved within 4 seconds.

The red and purple lines in the figures represent the responses with the largest initial errors. The lines both start at the same absolute lateral and course offset, but with opposite signs. Even though the errors have the same magnitude, the difference in settling time is significant. The purple line corresponds to the

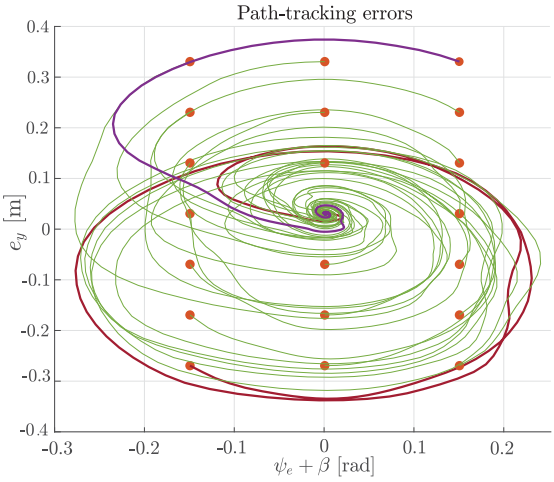

Fig. 8. Phase plot of the response of the vehicle to initial offsets in lateral position and orientation, showing how the path-tracking errors are resolved.

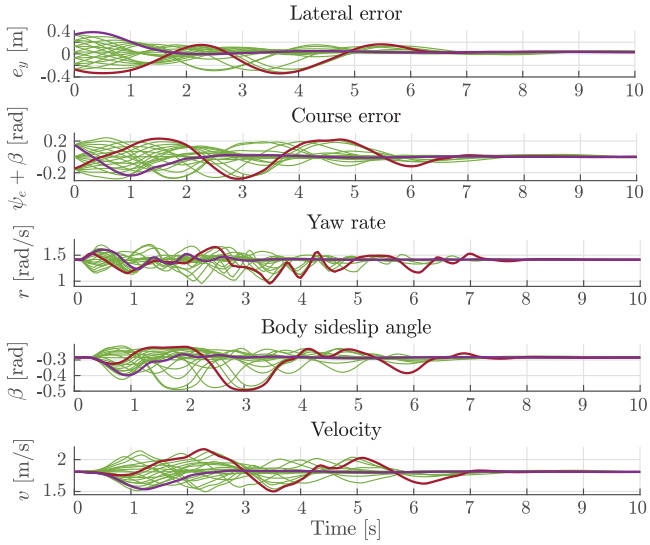

Fig. 9. Time response of the response of the vehicle to initial offsets in lateral position and orientation, showing how the path-tracking errors are resolved.

vehicle starting on the inside of the curve. This means that the vehicle will always move towards any part of the path. The red line corresponds to the vehicle driving on the outside of the circular path. This makes it more difficult for the controller to move towards the path, hence the longer settling time.

B. Initial Body Sideslip Angle and Yaw Rate Errors

To test the sensitivity to initial body sideslip and yaw rate errors, the vehicle is placed at various initial conditions corresponding to left-hand drift equilibria derived from the vehicle model. The results are shown in Fig. 10, where the red and purple line are indicating the most extreme initial condition offsets. From the figure it becomes apparent that the controller cannot solve all errors simultaneously. To increase the body sideslip angle of the purple response, the throttle is increased. This, however, also results in an increased velocity and the course

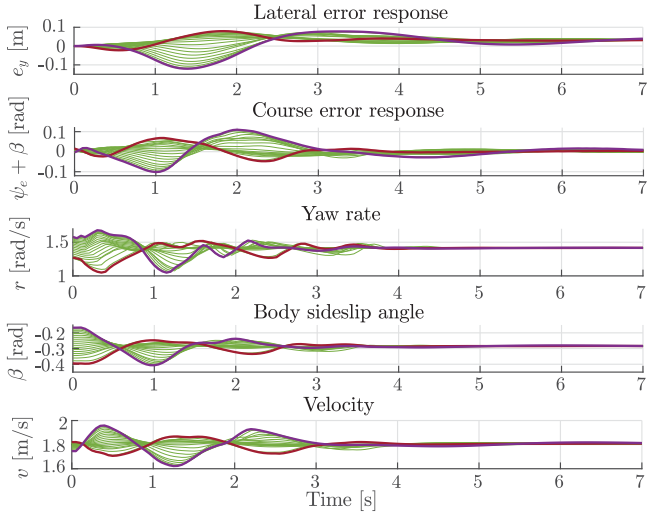

Fig. 10. Response of the drift controller to perturbations in body sideslip angle and yaw rate.

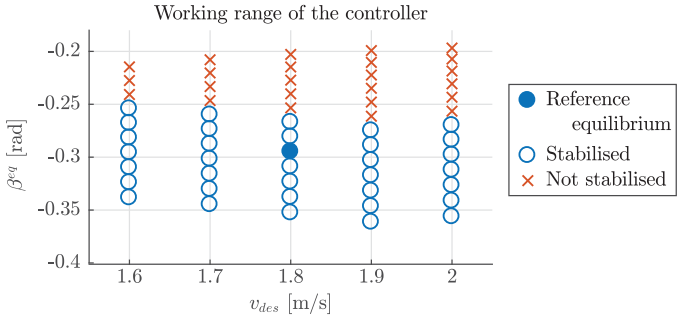

Fig. 11. Range of equilibria, around the tuned equilibrium, where the controller succeeds in stabilising the vehicle.

of the vehicle moving away from the path. To resolve the course error, the yaw rate has to remain large. As a result, a large overshoot in body sideslip angle can be observed. The red response already starts at a large body sidelip angle. By decreasing the throttle input, the yaw rate decreases and, subsequently, the body sideslip angle decreases. This, however, results in a much smaller velocity error, which makes it easier for the controller to resolve.

C. Performance Around Other Equilibria

Next, the controller performance is evaluated around other equilibria. From the equilibrium analysis in Section III, a range of left-hand drift equilibria is selected for velocities from 1.6 to 2 m/s, starting at the lowest equilibrium yaw rate. Fig. 11 shows for which equilibria the controller is able to stabilise the vehicle when tuned for the reference equilibrium (indicated by the solid blue dot in the figure).

The figure shows that the controller performs particularly well for large sideslip angles. Regarding stabilisation, this is indeed the case, since it is able to stabilize the vehicle for larger desired sideslip angles. The path-tracking performance, on the other hand, decreases for a larger body sideslip angle. For a body sideslip angle above -0.32 rad, a steady-state lateral error of

TABLE I
MEASURED AND ESTIMATED MODEL PARAMETERS OF THE DSV

Symbol	Value	Description
m	2.286 kg	Vehicle mass
R_e	0.0313 m	Effective wheel radius
t	0.1515 m	Axle track
ℓ	0.26 m	Wheelbase
I_z	0.04 kg $\cdot$ m^2	Initial estimate of the yaw moment of inertia
$C_{\alpha,f}$	13.82 N/rad	Front lateral tyre stiffness
$C_{\alpha,r}$	25.21 N/rad	Rear lateral tyre stiffness
$\sigma_{rl,lat}$	0.0144 m	Lateral relaxation length
C_σ	34.45 N/rad	Longitudinal tyre stiffness
μ_{max}	0.35	Tyre-road friction coefficient
$\sigma_{rl,long}$	0.04 m	Longitudinal relaxation length

below 5 cm is observed, which is acceptable. Below this sideslip angle, however, a significant increase in steady-state lateral error can be observed. The vehicle is stabilized at another equilibrium, with a lower velocity and a higher yaw rate. This is a results the mismatch between model and reality. The equilibrium is derived from a vehicle model, which does not perfectly align with the equilibria of the vehicle. The vehicle will therefore end up in a different equilibrium.

D. Parametric Robustness

The vehicle model used in this research is identified based on experiments with the scaled vehicle. This means that the found parameters are an estimation and differences between the actual vehicle and the vehicle model are present. In Fig. 12 a comparison between the identified vehicle model and vehicle measurements for the same inputs is shown. From this figure it becomes clear that although the results are comparable, there definitely are differences between the model and the actual vehicle.

The drift controller is based on the estimated vehicle properties and uses the same parameters as the vehicle model, of which the most important are shown in Table I. The tyre models used in the controller, for example, are based on the same tyre parameters. Because the controller is dependent on mostly the tyre model and friction, several tests are performed to find out how the controller copes with a $\pm 10\%$ change of the friction factor, and a $\pm 20\%$ change of the tyre stiffness. The controller is able to stabilise the vehicle for these parameter changes, but the performance degrades. In terms of velocity the controller copes very well with a 10% lower friction, a different drift equilibrium is found but the path-tracking errors are resolved completely. For a 10% higher friction, the yaw rate of the vehicle keeps varying in a sinusoidal motion with. The reason for this is that the controller 'expects' to reach the maximum lateral tyre force much sooner than it actually does, since a higher friction factor results in an increased lateral tyre force peak. The controller therefore does not increase the throttle input enough to reach the desired drift equilibrium. The cornering stiffness has an influence in the slope of the slip-force relationship. An increased cornering stiffness results in an increased slope, and vice versa. In other words, a change in wheel slip angle results in a larger increase in tyre force. The decreased cornering stiffness has a small influence on the vehicle response; the path-tracking errors

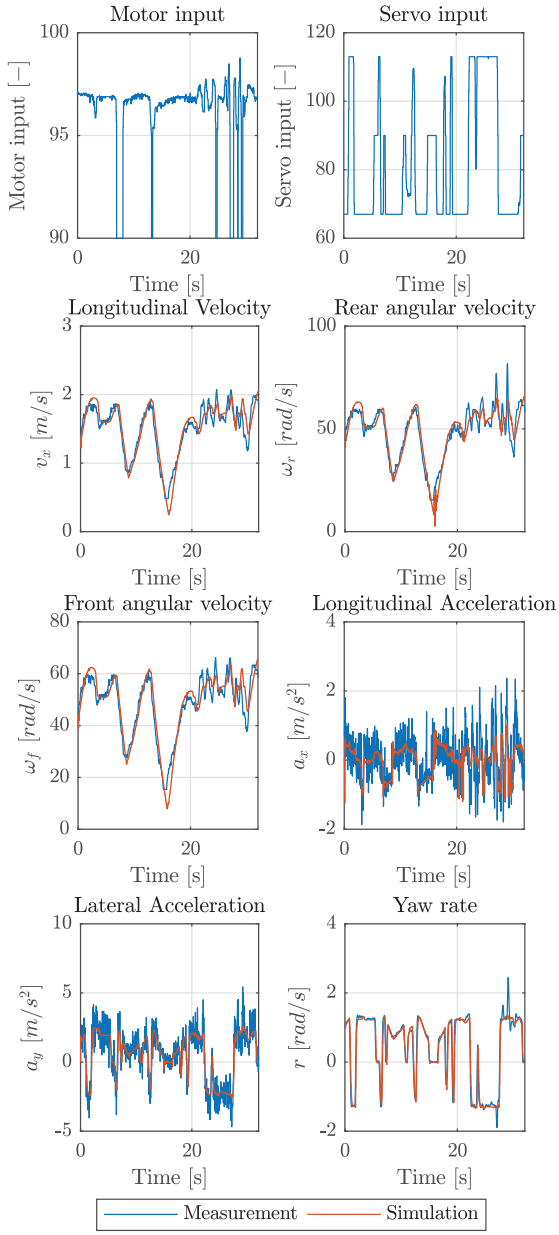

Fig. 12. Comparison between vehicle measurements and the vehicle model for varying throttle and steering inputs.

slightly increase. The effect of increasing the cornering stiffness is much larger. Because of the increased slope of the tyre force curve, a change in steering angle results in a larger increase or decrease in lateral tyre force than expected. This results in yaw rate and body sideslip oscillations. The controller is, however, still able to stabilise the vehicle around the path for the $\pm 20\%$ change of the tyre stiffness.

VII. SIMULATION

In simulation, the vehicle model can be initialised at a drift equilibrium. In an actual vehicle, however, this is not possible. The controller should, therefore, be able to transfer the vehicle from typical cornering conditions to drifting.

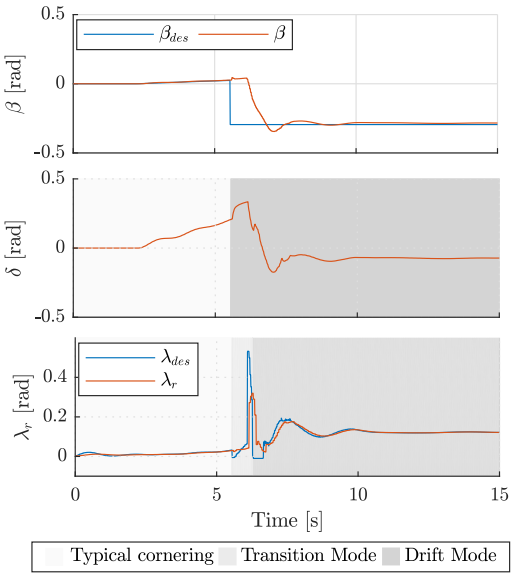

Fig. 13. The transition from straight-ahead driving to drifting in a circle.

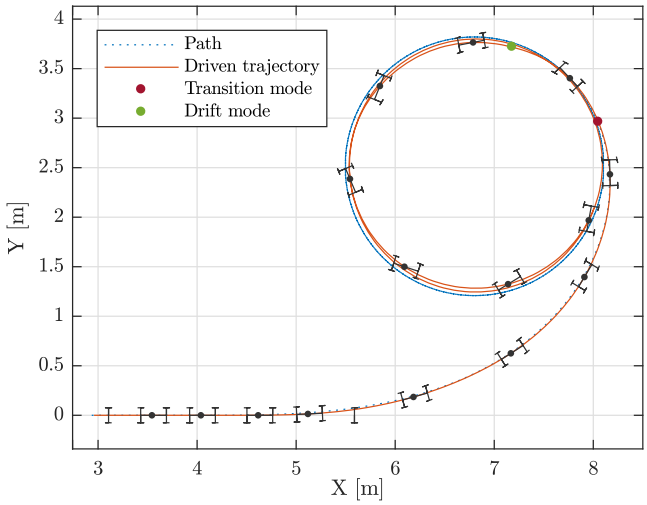

Fig. 14. Trajectory of the transition from straight-ahead driving to drifting in a circle.

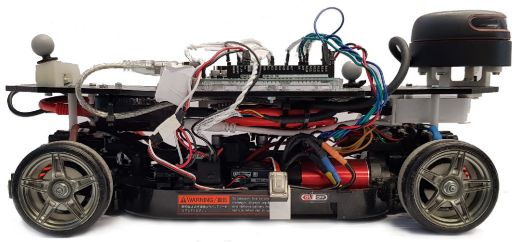

Fig. 15. The Delft Scaled Vehicle.

A drift can be entered as follows; first, a yaw motion is induced by steering into the corner. When the vehicle is rotating, the rear tyres are saturated to decrease the lateral tyre force. This is done by braking or a large throttle input. Because the rear lateral tyre force decreases, the rear-end of the vehicle starts sliding out of the curve. When nearing the desired body sideslip angle, the yaw rate is decreased by counter-steering and decreasing the throttle input.

The controller defined in this research, follows the same steps to induce a drift. However, by simply switching between the two controller modes, the vehicle moves away from the path. Therefore an intermediate step is introduced that intentionally steers to the inside of the curve, before increasing the throttle. This results in less deviation from the path.

In Fig. 13 the vehicle response is shown for the transition from straight-ahead driving to drifting in a circle. The driven trajectory is shown in Fig. 14. Before the vehicle reaches the final curvature, the controller switches to transition mode (indicated by the red dot in the trajectory plot). The vehicle starts steering into the corner, and after 0.5 s the throttle is increased. The drop in velocity is a result of the quickly increasing steering angle and the decreasing longitudinal velocity reference, that is coupled with the body sideslip angle. The same manoeuvre is tested for the velocities and equilibria as used in the sensitivity analysis. For the majority of the equilibria, the lateral error remains between ± 0.1 m and reaches steady-state within a few seconds.

VIII. Implementation

The final step of this research is the implementation of the drift controller in the Delft Scaled Vehicle, Fig. 15, a 1/10 scale radio controlled car, equipped with various sensors to measure accelerations, wheel speeds and location. The motion controller is developed in Matlab Simulink. Implementation in the scaled vehicle is performed by building the controller Simulink model as a ROS node. The scaled vehicle as an onboard computer on which the ROS network run. The chosen path is circular with a radius of 1.40 m. The reference velocity is chosen to be 1.7 m/s. The yaw rate is based on the velocity and curvature (1.21 rad/s), and the body sideslip angle is obtained from the corresponding drift equilibrium (-0.4 rad). Finally, some adjustments to the controller gains are made, to improve the performance in this application. The used controller gains are shown in Table II. In Fig. 16 the path of the scaled vehicle in a successful drifting manoeuvre is shown. The states, path-tracking errors and control inputs during a drifting manoeuvre are shown in Fig. 17.[1]

TABLE II
Controller Gains of the Implemented Drift Controller

Controller gain	Value	Controller gain	Value
K^d_β	5.8	t^d_{la}	1.2
K^d_r	2.8	t_t	0.2s
$K^d_{v,t}$	0.4	$\lambda_{des,t}$	0.35
$K^d_{\beta,t}$	3.3	$K^d_{r,t}$	0.6

Initially, the vehicle drives in typical cornering conditions. After a few seconds, the controller saturates the rear tyres and induces the drift. The controller is able to maintain the drift, with the body sideslip angle close to its reference value. The

[1] A video of the implemented drift controller can be found at https://youtu.be/VWgdd5jgyuk

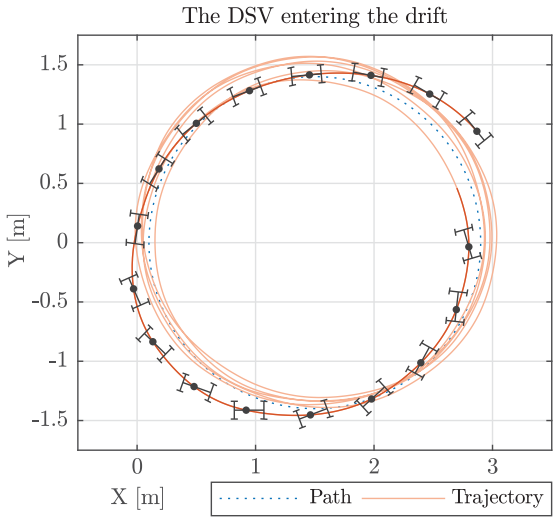

Fig. 16. Driven trajectory during a drifting manoeuvre with the DSV.

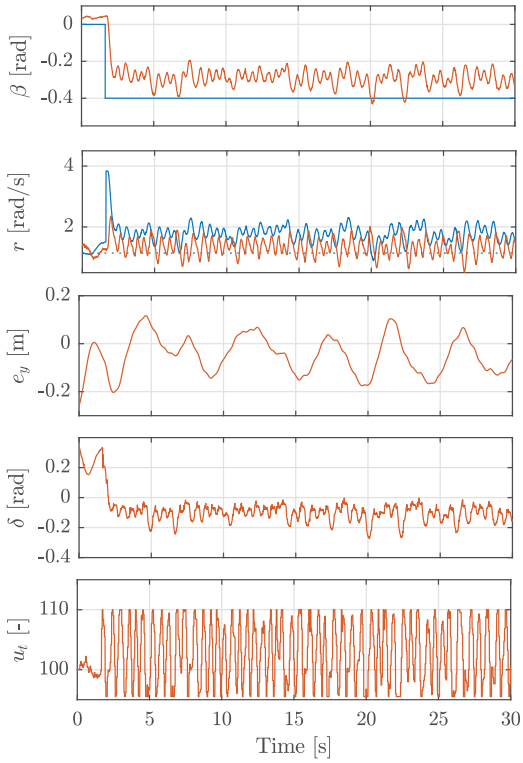

Fig. 17. States, path-tracking errors and control inputs during a drifting manoeuvre with the DSV.

lateral and course error show large oscillations with a period of approximately 5 seconds. An explanation for these oscillations can be found in the trajectory plot. Initially, the vehicle drives in typical cornering conditions towards the path. When the drift is induced, the vehicle first moves away from the path. It then crosses the path to, eventually, settle at a somewhat constant circular motion. The radius of this circle, however, is slightly larger than the radius of the path and it is translated a few centimetres in the positive Y direction. The latter results in the periodical variations in the lateral and course error and the period of approximately 5 seconds originates from the time it takes for the vehicle to make one circumference. So even though the course and lateral error show large variations, a somewhat constant circular motion can be observed.

Additionally, higher frequency oscillations in the states can be observed. These oscillations result from the various lags in the system. These oscilations originate from the lag in the system and low resolution of the throttle input, resulting in a oscillating throttle input. These oscillations carry through to the other vehicle states.

IX. Conclusion

In this research an extension to a drift controller is proposed to add path tracking capabilities. A desired yaw rate is based on the path-tracking errors and velocity and used as an input for the drift controller. This allows the controller to keep the vehicle close to the path while drifting. A sensitivity analysis shows that the controller can stabilise the drifting vehicle around the path for various curvatures and velocities. Additionally, it showed the controller can stabilise the vehicle from significant state perturbations. Furthermore, the controller is able to enter a drift from typical cornering conditions. By steering into the corner, before saturating the rear tyres, the deviation from the path during the transition can be minimised. The controller is implemented in a 1/10 scaled vehicle, which it achieved to bring into a drift and sustain it, while remaining close to the path. Still, additional work is recommended on the following points. Firstly, the controller is highly dependent on the equilibrium analysis, from which the reference body sideslip angle is directly obtained. Due to model mismatches, this equilibrium body sideslip angle does not necessarily correspond to the same curvature for the actual vehicle. It is therefore recommended to find an alternative method of determining the reference body sideslip angle or add additional feedback to resolve the model mismatches. Furthermore, the model currently uses static feedback gain, this makes the controller simple but also optimised around a specific equilibrium. To make the controller applicable over a wider range of drift equilibria some sort of gain scheduling could be added. Furthermore, to reduce the oscillations in the throttle input in the scaled vehicle, the wheel slip controller and possibly the drivetrain of the scaled vehicle should be improved. The oscillations occured because of the lag in the system and the large influence of the state of charge of the battery on the motor performance.

Finally, the scaled vehicle is modelled by vehicle dynamics of a full-scaled vehicle, and the tyres are modelled using the Dugoff tyre model. Though the proposed method adds path-tracking capabilities to a drift controller which its performance is proven on a full-scaled vehicle, since the tyres on the scaled vehicle differ a lot from tyres on full-scaled vehicles, it is difficult to draw a conclusion about the absolute performance of the proposed controller. To get a better understanding of the absolute controller performance, a more thorough analysis of the tyre behaviour by implementation on a full-scaled vehicle is considered as future work.

REFERENCES

[1] R. Y. Hindiyeh, "Dynamics and control of drifting in automobiles," Ph.D. dissertation, Stanford University, 2013.

[2] D. Brdos, Z. Szalay, V. Tihanyi, and L. Palkovics, "MIMO controller design for stabilizing vehicle drifting," in *Proc. IEEE 19th Int. Symp. Comput. Intell. Informat. 7th Int. Conf. Recent Achievements Mechatronics, Automat., Comput. Sci. Robot.*, 2019, pp. 000187–000192.

[3] E. Joa, H. Cha, Y. Hyun, Y. Koh, K. Yi, and J. Park, "A new control approach for automated drifting in consideration of the driving characteristics of an expert human driver," *Control Eng. Pract.*, vol. 96, 2020, Art. no. 104293.

[4] A. Arab, K. Yu, J. Yi, and Y. Liu, "Motion control of autonomous aggressive vehicle maneuvers," in *Proc. 2016 IEEE Int. Conf. Advanced Intelligent Mechatronics (AIM)*, pp. 1663–1668, 2016.

[5] E. Wachter, A. Schmeitz, F. Bruzelius, and M. Alirezaei, "Path control in limits of vehicle handling: A sensitivity analysis," in *Advances in Dynamics of Vehicles on Roads and Tracks. IAVSD 2019*. Cham, Switzerland: Springer, 2020, pp. 1089–1095.

[6] E. Wachter, M. Alirezaei, F. Bruzelius, and A. Schmeitz, "Path control in limit handling and drifting conditions using state dependent riccati equation technique," *Proc. Inst. Mech. Eng., Part D: J. Automobile Eng.*, vol. 234, no. 2/3, pp. 783–791, Feb. 2020.

[7] M. Baars, "Modelling and control of a scaled car in and beyond stable limit handling," Master thesis, Delft Univ. Technol., Delft, The Netherlands, 2018.

[8] J. Y. Goh, T. Goel, and J. Christian Gerdes, "Toward automated vehicle control beyond the stability limits: Drifting along a general path," *J. Dyn. Syst., Meas., Control*, vol. 142, 2019. Art. no. 021004.

[9] H. Baars, M. Hellendoorn, and M. Alirezaei, "Control of a scaled vehicle in and beyond stable limit handling," in *Adv. Dyn. Veh. Roads Tracks* M. Klomp, F. Bruzelius, J. Nielsen, and A. Hillemyr, Eds. Cham, Switzerland: Springer Int., 2020, pp. 1121–1128.

[10] P. Hingwe and M. Tomizuka, "A variable look-ahead controller for lateral guidance of four wheeled vehicles," in *Proc. Amer. Control Conf.*, vol. 1, Jun. 1998, pp. 31–35 .

[11] S. Patwardhan, H.-S. Tan, and J. Guldner, "A general framework for automatic steering control: System analysis," in *Proc. Amer. Control Conf. (Cat. No.97CH36041)*, 1997, vol. 3, pp. 1598–1602.

[12] N. R. Kapania and J. C. Gerdes, "Design of a feedback-feedforward steering controller for accurate path tracking and stability at the limits of handling," *Veh. Syst. Dyn.*, vol. 53, no. 12, pp. 1687–1704, 2015.

[13] A. Schmeitz, J. Zegers, J. Ploeg, and M. Alirezaei, "Towards a generic lateral control concept for cooperative automated driving," in *Proc. 5th IEEE Int. Conf. Models Technol. Intell. Transp. Syst.*, 2017, pp. 134–139.

[14] K. M. Kritayakirana, "Autonomous vehicle control at the limits of handling," Ph.D. dissertation, Stanford Univ., Stanford, CA, USA, 2012.

Mart Baars received the M.E. and master's degree in systems and control from the Delft University of Technology, Delft, The Netherlands, in 2018. He is currently a Vehicle Control Engineer with the Department of Integrated Vehicle Safety, TNO, Helmond, The Netherlands. His research interests include the development, integration, testing of vehicle control systems, and advanced driver assistance systems.

Hans Hellendoorn received the Ph.D. degree in computer science from the Delft University of Technology (TU Delft), Delft, The Netherlands, in 1990. Until 2008, he was with Siemens Research, Munich, Germany and Siemens, The Netherlands. From 1999 to 2008, he was a part-time Professor of industrial applications of computational intelligence. Since 2008, he has been a full-time Professor of control theory. From 2012 to 2018, he was the Chair of the Delft Center for Systems and Control, since April 2018, he has been Chair of the Cognitive Robotics Department. His research focuses on multiagent control of large-scale hybrid systems. Besides research he is active in education. From 2011 to 2021, he was the Director of Education and the Graduate School with faculty 3mE, since 2021, he has been a Pro Vice Rector Magnificus for Joint Education with TU Delft. He is the co-author of four scientific books and author and coauthor of more than 200 scientific publications. He has supervised more than 100 MS.c. students and more than 20 Ph.D. students.

Mohsen Alirezaei received the Ph.D. degree in mechanical engineering, robotics and control from the Delft University of Technology, Delft, The Netherlands, in 2011. In 2012, he was a Postdoc Researcher with the Delft University of Technology. He was a Senior Scientist with Integrated Vehicle Safety Department, TNO automotive during 2012–2019 and a part time Assistant Professor with the Delft University of Technology during 2015–2019. He is currently a Fellow Scientist with Siemens Industry Software and Services, Helmond, The Netherlands and a part time Assistant Professor with the Eindhoven University of Technology, Eindhoven, The Netherlands. His research interests include verification and validation of automated and cooperative automated driving and advance driver assistance systems.